Dalton Transactions

ROYAL SOCIETY OF CHEMISTRY

PAPER

View Article Online
View Journal | View Issue

Cite this: *Dalton Trans.*, 2026, **55**, 6120

Formation of calcium-phosphate-based supra-ceramics in solutions containing glutaric acid derivatives

Taishi Yokoi * and Masakazu Kawashita

Octacalcium phosphate (OCP) can incorporate specific carboxylic acids into its crystal lattice. Such substances accomodating a molecular component in their crystal lattice have been recently categorised as supra-ceramics. However, the physicochemical properties that govern the ability of carboxylic acids to be incorporated into the OCP crystal are unknown. In this study, OCP was synthesised in aqueous solutions of glutaric acid and its derivatives, each with different dissociation constants. Synthesis experiments were conducted to determine whether these carboxylic acids can be incorporated into OCP. Glutaric acid, iminodiacetic acid, and diglycolic acid could be incorporated into OCP, whereas 2,2′-thiodiglycolic acid was not incorporated into OCP, revealing for the first time that iminodiacetic acid and diglycolic acid can be incorporated into OCP. In addition, the dissociation constant of 2,2′-thiodiglycolic acid, which could not be incorporated, had an intermediate value among the studied carboxylic acids, suggesting that the dissociation constant of carboxylic acids is unlikely to be a factor governing their ability to be incorporated into OCP. These findings are expected to contribute to a deeper understanding of the incorporation of carboxylate ions into the OCP crystal.

Received 18th December 2025,
Accepted 26th March 2026

DOI: 10.1039/d5dt03031e

rsc.li/dalton

Introduction

Inorganic layered compounds are an essential class of compounds, which, due to their fundamental scientific importance and wide range of applications as biomedical, energy, electrical, optical, and magnetic materials, as well as catalysts, have attracted intense research interest.[1–10] The incorporation of different molecules and ions between the layers is a fascinating structural property of these compounds that plays a key role in determining their functional characteristics. Octacalcium phosphate (OCP, $Ca_8(HPO_4)_2(PO_4)_4{\cdot}5H_2O$) has a layered structure composed of apatitic and hydrated layers,[11,12] where the hydrogen phosphate ions in the hydrated interlayer can be substituted by carboxylate ions,[13,14] which, in most cases, are dicarboxylate ions.[15–24] Among tricarboxylic acids, only citric acid has reportedly been incorporated into OCP,[25,26] whereas among tetracarboxylic acids, 1,2,4,5-benzenetetracarboxylic acid has been reported to be incorporated into OCP.[27] Recently, Maeda *et al.* introduced a novel category for inorganic solids incorporating molecular units called supra-ceramics.[28] Based on this definition, carboxylate-containing OCP can be regarded as a supra-ceramic.

Recent research on OCP incorporating carboxylate ions has focused on developing new materials, particularly fluorescent materials. OCPs incorporating aromatic carboxylate ions exhibit fluorescence[29–32] and are expected to be used as bioimaging probes in the future. OCP is considered a precursor of bone apatite[33] and is also actively studied as an artificial bone[34–44] alongside carbonate apatite.[45–53] In other words, OCP is a biocompatible material and a candidate for biomedical applications, including bioimaging probes. However, developing OCP-based materials with incorporated carboxylate ions must overcome a significant challenge posed by OCP's guest selectivity. For a given proposed novel OCP with incorporated carboxylate ions, it is currently impossible to know in advance whether the carboxylic acid can be incorporated into the OCP; rather, this can only be determined by experimental synthesis, hindering the rapid exploration of numerous possible carboxylate-ion-incorporating OCP systems. Hence, elucidation of the underlying mechanism of guest selectivity in OCP is expected to accelerate the development of OCP materials incorporating carboxylate ions dramatically.

The guest selectivity of OCP is not only a function of the size of the carboxylic acid but also depends on the fine details of its molecular structure, as illustrated by the following example. Adipic acid ($HOOC(CH_2)_4COOH$) is a typical car-

Laboratory for Biomaterials and Bioengineering, Institute of Integrated Research, Institute of Science, Tokyo, 2-3-10 Kanda-Surugadai, Chiyoda-ku, Tokyo 101-0062, Japan. E-mail: yokoi.taishi.bcr@tmd.ac.jp

boxylic acid that can be incorporated into OCP, and its structure and size are similar to those of *cis*,*cis*-muconic acid (HOOCCH=CHCH=CHCOOH), which can also be incorporated into OCP. By contrast, it was reported that *trans*,*trans*-muconic acid (HOOCCH=CHCH=CHCOOH) cannot be incorporated into OCP,[54] demonstrating that small changes in molecular structure can strongly affect the carboxylic acid's ability to be incorporated into OCP. Although achieving such guest selectivity usually requires a precisely tuned host structure, OCP exhibits guest selectivity without such structural control. To date, the mechanism underlying OCP's guest selectivity remains poorly understood.

The physicochemical parameters of carboxylic acids, including molecular size, molecular weight, molecular conformation, stability constant of their complex with calcium ions, and dissociation constant, can vary significantly. It is desirable to vary only a single parameter when investigating the influence of these factors on OCP incorporation; however, conducting such an experiment in practice is difficult. However, our preliminary investigation found that for glutaric acid (GA, $HOOC(CH_2)_3COOH$) and its derivatives, the dissociation constant changes systematically, whereas the molecular size remains nearly constant. Therefore, we expect that the effect of the dissociation constant of carboxylic acids on their incorporation into OCP can be elucidated by examining the incorporation behaviour of these carboxylic acids. In this study, we investigated the incorporation behaviour of GA and its derivatives into OCP to determine whether the dissociation constant is the dominant factor governing incorporation.

Experimental section

Synthesis

The OCP samples were synthesised through a reaction using calcium carbonate and phosphoric acid in the carboxylic acid solutions. GA, iminodiacetic acid (IDAA, $HOOCCH_2NHCH_2COOH$), diglycolic acid (DGA, $HOOCCH_2OCH_2COOH$), and 2,2′-thiodiglycolic acid (TDGA, $HOOCCH_2SCH_2COOH$) were used in this study. The molecular structures of these carboxylic acids are shown in Fig. 1. The synthesis of OCP samples is described in detail in the SI. The sample name is defined as *X*–*Y*, where *X* indicates the carboxylic acid used for OCP synthesis, namely GA, IDAA, DGA, or TDGA, and *Y* indicates the amount (mmol) of carboxylic acid used for the sample synthesis. For instance, IDAA-25 refers to the sample synthesised using 25 mmol of IDAA.

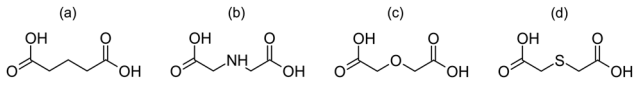

Fig. 1 Molecular structures of (a) glutaric acid (GA), (b) iminodiacetic acid (IDAA), (c) diglycolic acid (DGA), and (d) 2,2′-thiodiglycolic acid (TDGA).

The OCP sample that did not contain carboxylate ions was synthesised as the standard material through the reaction between calcium carbonate and phosphoric acid mixed in ultrapure water, and is denoted as CONTROL.

Characterisation

The crystal phases of the samples were determined by X-ray diffraction (XRD, MiniFlex600, Rigaku Corp. Ltd, Tokyo, Japan) using Cu-Kα radiation (0.154 Å), based on the powder diffraction file (PDF). Fluorophlogopite (Topy Industries Ltd, Tokyo, Japan) was added as an internal standard before XRD measurements to determine the (100) interplanar spacing (d_{100}) of the samples. The fluorophlogopite : sample mass ratio was fixed at 1 : 4, and the OriginPro 2025 software was used for peak separation. The chemical structures of the samples were characterised by attenuated total reflection Fourier-transform infrared (FTIR) spectroscopy (FT/IR-6200, JASCO Corp., Tokyo, Japan) using a Ge prism and Raman spectroscopy (WP 785X-R, Wasatch Photonics Inc., UT, USA) using a 785 nm laser. Thermogravimetry (TG) and differential thermal analysis (DTA) were performed for representative samples using a thermal analyser (DTG-60H, Shimadzu Corp., Kyoto, Japan).

The stable structures of GA, IDAA, DGA, and TDGA in vacuum were estimated using the universal force field method[55] and the Avogadro software (Ver. 1.2.0).[56] The molecular size was obtained from the stable structures. The dissociation constants (pK_{a1} and pK_{a2}) of these dicarboxylic acids were estimated using MarvinSketch (Ver. 23.11.0) for an ionic strength of 0.1 mol L^{-1} at 25 °C.

Results

We have formerly demonstrated the successful synthesis of OCP with incorporated glutarate ions (GA-25), and since these results have been described previously,[20] they will not be described in detail here. However, because the d_{100} value obtained for GA-25 by XRD analysis is discussed below, the XRD pattern of GA-25 is included in the SI (Fig. S1).

OCP synthesised in IDAA solution

The XRD patterns of the samples synthesised in the IDAA solution are shown in Fig. 2(a). The diffraction peaks detected in CONTROL can be assigned to plain OCP ($Ca_8(HPO_4)_2(PO_4)_4 \cdot 5H_2O$, PDF #01-074-1301). Hereafter, the term "plain OCP" will be used to distinguish it from OCP with incorporated carboxylate ions. The OCP phase was detected in IDAA-1, IDAA-5, IDAA-10, and IDAA-25, with no other phases observed. The 100 diffraction peak at approximately 5° in IDAA-1, IDAA-5, and IDAA-10 was detected at the same position as that in CONTROL, whereas the 100 diffraction peak in IDAA-25 appeared to be shifted slightly to a lower 2θ angle relative to the 100 diffraction peak of CONTROL. Fig. 2(b) shows the XRD pattern measured for an angle-standard material (fluorophlogopite) added to accurately examine the peak positions. The two diffraction peaks of IDAA-25 were detected at lower angles

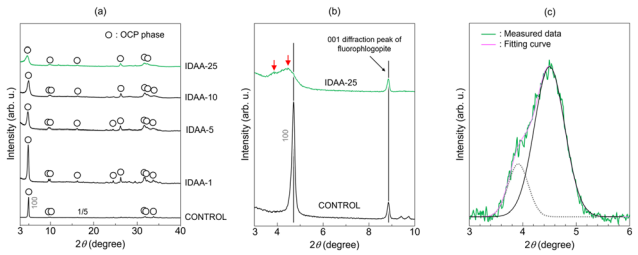

Fig. 2 (a) XRD patterns of OCP synthesised in IDAA solution. (b) Comparison of XRD patterns of CONTROL and IDAA-25 mixed with fluorophlogopite used as the angular standard material. (c) Peak fitting result for the diffraction peak of IDAA-25 in the 3–6° range. The red arrows in (b) indicate the 100 diffraction peaks in the XRD pattern of IDAA-25.

than the peak of the 100 diffraction of CONTROL. The d_{100} of CONTROL was calculated to be 1.87 nm according to Bragg's law, because the 100 diffraction of CONTROL was detected at 4.71°. The signal-to-noise ratio of the XRD pattern of IDAA-25 (Fig. 2(b)) was not sufficiently high to determine the peak positions accurately. Therefore, peak fitting was performed for the XRD pattern of IDAA-25, with the results shown in Fig. 2(c). The peak positions were 3.88° and 4.46°, and the d_{100} values calculated using Bragg's law from these diffraction angles were 2.27 nm and 1.98 nm, respectively.

The FTIR and Raman spectra of CONTROL and IDAA-25 are shown in Fig. 3. The observed FTIR and Raman peaks were assigned based on a previous report by Marković *et al.*[57] Clear FTIR absorption peaks were detected at 917, 961, 1024, 1039, 1056, 1078, 1102, 1121, 1193, and 1646 cm^{-1} for CONTROL. Except for the peak detected at 1646 cm^{-1}, these peaks were assigned to phosphate species. In particular, the absorption peak detected at 1193 cm^{-1} was attributed to hydrogen phosphate ions present in the OCP interlayer. The peak detected at 1646 cm^{-1} was assigned to H_2O bending vibration. Compared with CONTROL, IDAA-25 showed broad peaks in its FTIR spectrum, with clear absorption peaks detected at 963, 1038, 1112, 1324, 1417, and 1627 cm^{-1}. In contrast to CONTROL, no absorption peak was detected at 1193 cm^{-1} for IDAA-25. The peaks at 963, 1038, and 1112 cm^{-1} were assigned to phosphate species, whereas the peak at 1324 cm^{-1} was assigned to CH_2 wagging, and that at 1417 cm^{-1} was attributed to COO stretching and CH_2 bending. The peak detected at 1627 cm^{-1} was assigned to H_2O bending. For CONTROL, Raman peaks were detected at 429, 450, 577, 591, 610, 878, 916, 960, 1011, 1048, 1088, 1114, and 1193 cm^{-1}, which were assigned to phosphate species. In comparison, the Raman spectrum of IDAA-25 was broader, with the peaks derived from COO stretching and CH_2 bending detected at 1419 and 1450 cm^{-1}, respectively.

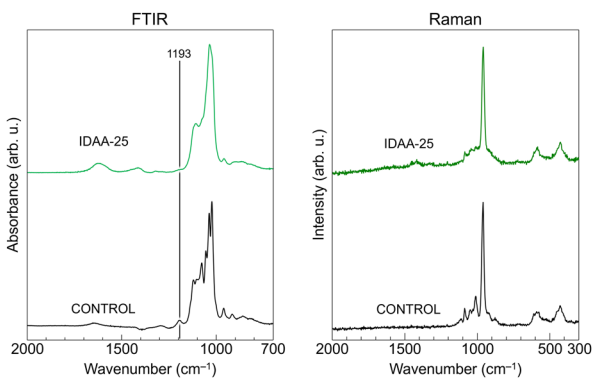

Fig. 3 FTIR and Raman spectra of CONTROL and IDAA-25.

OCP synthesised in DGA solution

The XRD patterns of the samples synthesised in the DGA solution are shown in Fig. 4(a). The OCP phase was detected in DGA-0.5, DGA-1, DGA-5, and DGA-10, and no other phase was detected. Two 100 diffraction peaks were detected at approximately 5° for DGA-0.5, whereas only a single 100 diffraction peak was detected for DGA-1, DGA-5, and DGA-10. In addition, the 100 diffraction peaks in DGA-1, DGA-5, and DGA-10 were shifted slightly to lower 2θ angles relative to the 100 diffraction peak of CONTROL. Fig. 4(b) shows the XRD pattern measured with an angle standard material (fluorophlogopite) added to accurately evaluate the peak positions. The 100 diffraction peak of DGA-10 was located at a lower 2θ angle than the 100 diffraction peak of CONTROL. In addition, a small shoulder was detected in the 100 diffraction peak of DGA-10. Peak fitting was performed for the XRD pattern of DGA-10 due to the presence of two 100 diffraction peaks in DGA-10, and the results are shown in Fig. 4(c). The positions of the two fitted peaks were 4.07° and 4.20°, and the d_{100} values obtained from these diffraction angles were 2.17 nm and 2.10 nm, respectively.

The FTIR spectra of CONTROL and DGA-10 are shown in Fig. 5. The assignments of the peaks in CONTROL are already described above; hence, they will not be repeated here. Clear absorption peaks were detected for DGA-10 at 908, 960, 1034, 1042, 1080, 1108, 1318, 1412, 1438, 1599, and 1637 cm^{-1}, matching the peaks observed in the CONTROL spectrum. However, the absorption peak at 1193 cm^{-1} detected in CONTROL was not detected in DGA-10. The peaks at 908, 960, 1034, 1042, 1080, and 1108 cm^{-1} were attributed to phosphate

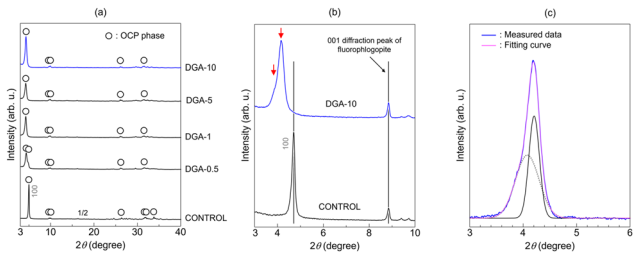

Fig. 4 (a) XRD patterns of OCP synthesised in DGA solution. (b) Comparison of XRD patterns of CONTROL and DGA-10 mixed with fluorophlogopite used as the angular standard material. (c) Peak fitting result for the diffraction peaks of DGA-10 in the 2θ range of 3–6°. The red arrows in (b) indicate 100 diffraction peaks in the XRD pattern of DGA-10.

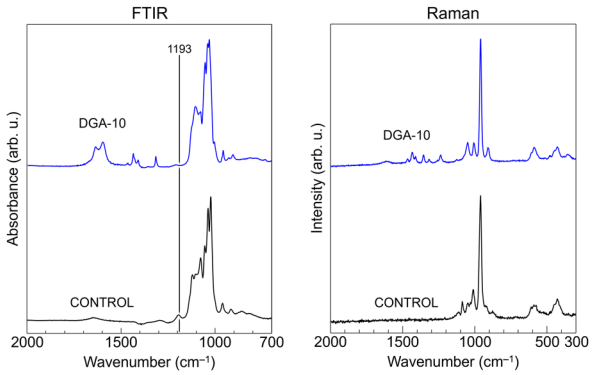

Fig. 5 FTIR and Raman spectra of CONTROL and DGA-10.

species. The absorption peak detected at 1318 cm^{-1} was assigned to CH_2 wagging, and the peaks at 1412 and 1438 cm^{-1} were attributed to COO stretching and CH_2 bending, respectively. The peak detected at 1599 cm^{-1} was assigned to COO stretching. The peak detected at 1637 cm^{-1} was identified as H_2O bending. In addition to the peaks observed in CONTROL, the Raman spectrum of DGA-10 showed several small peaks in the 1500–1200 cm^{-1} range. Except for the peak at 1317 cm^{-1} derived from HPO_4, these peaks were assigned to the COO and CH_2 moieties of DGA incorporated into OCP.

OCP synthesised in TDGA solution

Fig. 6(a) shows the XRD patterns of samples synthesised in the TDGA solution. The OCP phase was detected in all samples. No impurity phases such as calcium carbonate, used as a starting material, were detected in TDGA-1, TDGA-5, TDGA-10, TDGA-15, and TDGA-20. Unlike in IDAA and DGA, no change in the 100 diffraction peak position was observed in these samples. TDGA-20 was selected as a representative sample, and the XRD patterns in which the positions of the diffraction peaks were corrected using the fluorophlogopite angular standard are shown in Fig. 6(b). The 100 diffraction peaks of CONTROL and TDGA-20 were both located at 4.71°. In addition, although two 100 diffraction peaks derived from the OCP phase were detected in IDAA-25 (Fig. 2(c)) and DGA-10 (Fig. 4(c)), only one 100 diffraction peak was detected in TDGA-20.

Fig. 7 shows the FTIR spectra of CONTROL and TDGA-20. The FTIR spectrum of TDGA-20 was similar to that of CONTROL, although showing slightly broader peaks compared with those of CONTROL. Absorption peaks at 915, 963, 1026, 1039, 1053, 1076, 1109, 1121, 1193, and 1642 cm^{-1} were detected in TDGA-20. With the exception of the peak at 1642 cm^{-1}, these peaks were derived from phosphate species, whereas the peak at 1642 cm^{-1} was attributed to H_2O bending. TDGA-20 exhibited a broader Raman spectrum than CONTROL, although the peak positions were almost the same. Moreover, the peak intensity of HPO_4 and PO_4 stretching at 1088 cm^{-1} was weaker.

Thermal analysis of representative samples

Fig. 8 shows the TG-DTA curves of CONTROL, IDAA-25, DGA-10, and TDGA-20. CONTROL, IDAA-25, and TDGA-20 exhibited a stepwise weight loss with a concurrent endothermic reaction up to 300 °C owing to dehydration of crystalline water in OCP. Above 300 °C, no significant endothermic or exothermic reaction was observed. The weight losses from 30 to 1000 °C were 14.5%, 17.2%, and 12.6% for CONTROL, IDAA-25, and TDGA-20, respectively. Simultaneous weight loss and an endothermic reaction was also observed for DGA-10 up to 300 °C because of dehydration of crystalline water. Additionally, a reaction was detected in the range of 300–800 °C, although it was difficult to determine whether it is endothermic or exothermic because the peaks in the DTA curve were small. Furthermore, the nature of the reaction can be reversed depending on how the background is taken. A weight loss of 4.3% occurred at approximately 850 °C, accompanied by an exothermic reaction. This weight loss is most likely due to decomposition of DGA in OCP. The total weight loss from 30 to 1000 °C was 23.5%.

Discussion

It was previously reported that glutarate ions can be incorporated into OCP. IDAA, DGA, and TDGA are GA derivatives, and

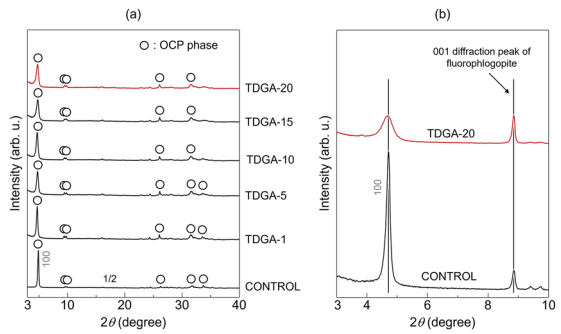

Fig. 6 (a) XRD patterns of OCP synthesised in TDGA solution. (b) Comparison of XRD patterns of CONTROL and DGA-20 mixed with fluorophlogopite used as the angular standard material.

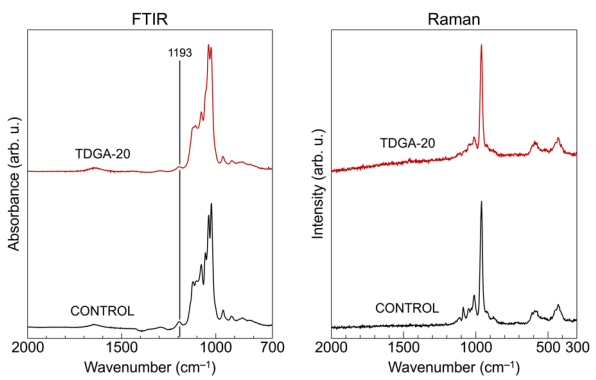

Fig. 7 FTIR and Raman spectra of CONTROL and TDGA-20.

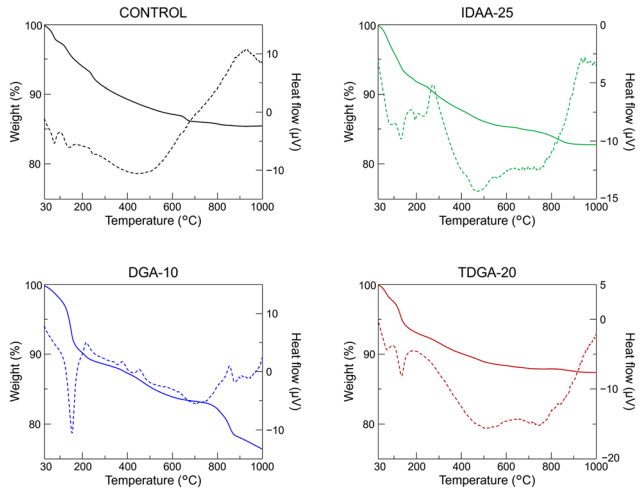

Fig. 8 TG-DTA curves of CONTROL, IDAA-25, DGA-10, and TDGA-20. The solid and dotted lines indicate weight and heat flow, respectively.

we discuss the incorporation of these dicarboxylate ions into OCP. The incorporation of carboxylate ions into OCP was confirmed by the expansion of the d_{100} of the OCP phase observed by XRD analysis, the detection of absorption bands derived from the carboxylate ion species, the reduced intensity of the FTIR absorption band derived from the hydrogen phosphate ions located in the OCP interlayers, and the detection of carboxylate ion moieties in the Raman spectra. For IDAA, the d_{100} values of IDAA-25 were 2.27 nm (minor phase) and 1.98 nm (main phase), and both values were larger than that of CONTROL (d_{100} = 1.87 nm) (Fig. 2). In addition, carboxylate ion moieties (COO and CH_2) were detected in the FTIR and Raman spectra of IDAA-25, and the absorption band of hydrogen phosphate ions located in the OCP interlayers showed reduced intensity in the FTIR spectrum (Fig. 3). This implies that IDAA can be incorporated into OCP, although a few studies have reported OCP systems exhibiting two 100 diffraction peaks. Applying similar criteria to other carboxylic acids, it can be determined that DGA was also incorporated into OCP (Fig. 4 and 5), whereas TDGA was not incorporated into OCP (Fig. 6 and 7). The amount of carboxylate ions incorporated into the OCP crystal was estimated to be larger for DGA than for IDAA, based on the weight loss from 30 to 1000 °C (Fig. 8).

The d_{100} values of OCP with incorporated dicarboxylate ions were strongly related to the molecular size of the incorporated dicarboxylate ions. We propose that the relationship between d_{100} and molecular size can be expressed using the following equation:[58]

$$d_{100} = 0.9355L + 1.7669\ (\mathrm{nm}) \quad (1)$$

where L is a parameter that represents the molecular size, specifically, the distance between the carbon atoms of the carboxy groups of the dicarboxylic acid. The linear relationship between the d_{100} value and molecular size L is reasonable because the main chain of the incorporated dicarboxylic acids is assumed to be parallel to the a-axis direction of the OCP crystal lattice. In other words, steric structures of carboxylate ions between the OCP interlayers can be estimated by comparing the d_{100} derived from the experimental XRD results (d_{100}(exp.)) with the d_{100} calculated using the equation proposed by our group (d_{100}(cal.)). The steric structures of carboxylate ions incorporated in the OCP crystal lattice are evaluated using such an indirect method because it is technically quite difficult to directly determine these steric structures.

Table 1 shows the L values of GA, IDAA, DGA, and TDGA, as well as d_{100}(exp.) and d_{100}(cal.) of OCP systems that incorporate these dicarboxylate ions. In addition, the $\Delta d_{100}/L$ values were calculated and are presented in Table 1. This parameter can be used as a measure of the likelihood of the incorporation of the dicarboxylate ions into OCP as follows: for the OCP crystal structure, d_{100} is the sum of the thicknesses of the apatitic and the hydrated layers. Hence, the difference between the experimental and calculated d_{100} values (Δd_{100} = d_{100}(exp.) − d_{100}(cal.)) is equivalent to the difference between the experimental and calculated thickness of the hydrated layer because the thickness of the apatitic layer can be regarded as independent of dicarboxylate ion incorporation. Because the thickness of the hydrated layer is determined by the size of dicarboxylate ions incorporated into the OCP interlayer, as measured by L, Δd_{100} measures the difference between the experimental (in other words, actual) and calculated L values of the dicarboxylic acid. When the absolute value of $\Delta d_{100}/L$ is sufficiently small, the carboxylate ions most likely exist between the OCP interlayers with the main chain parallel to the a-axis direction of the OCP crystal. This is because d_{100}(cal.) is calculated based on the assumption that the main chain of the dicarboxylate ions incorporated into the hydrated layers of OCP is parallel to the a-axis direction of the OCP crystal.

The calculated $\Delta d_{100}/L$ of GA was +9.8%. Although this value was slightly larger than the values for the previously reported dicarboxylate ions incorporated into OCP, glutarate ions likely existed in OCP with their main chain parallel to the a-axis direction. A positive $\Delta d_{100}/L$ value implies that the size of the incorporated carboxylic acid in OCP is larger than the calculated value. Hence, the C–C–C bonding angles in the main chain of incorporated glutarate ions were slightly larger than the calculated optimal values, and glutarate acted as a

Table 1 Summary of the L values of GA, IDAA, DGA, and TDGA, as well as d_{100}(exp.) and d_{100}(cal.) of OCP incorporating these dicarboxylate ions. The calculated $\Delta d_{100}/L$ values are also provided

Carboxylic acid	Experimental value d_{100}(exp.) (nm)	Calculated value L (nm)	d_{100}(cal.) (nm)	$\Delta d_{100}/L$ (%)
GA	2.29	0.506	2.240	+9.8
IDAA	1.98^{main}	0.490	2.225	−50.1
	2.27^{minor}			+9.1
DGA	2.10^{main}	0.476	2.212	−23.6
	2.17^{minor}			−8.9
TDGA	N/A	0.540	2.272	N/A

^{main}: main phase, ^{minor}: minor phase.

larger ion. Interesting phenomena were observed for IDAA and DGA. In both cases, the absolute value of $\Delta d_{100}/L$ calculated for the main phase was larger than that for the minor phase. This suggests that iminodicarboxylate ions and diglycolate ions do not mainly assume a linear structure between the OCP interlayers, and the linear structure of carboxylate ions in the OCP interlayers does not always appear to be the most stable; rather, these ions assume some kind of bent structure. Carboxylic acids with side chains, namely succinic acid derivatives, have been suggested to assume a bent structure;[58] hence, it is not surprising that iminodicarboxylate ions and diglycolate ions exhibit a bent structure in the OCP crystal. IDAA and DGA have nitrogen and oxygen atoms, respectively, in their main chain, which can form coordination bonds with calcium ions and hydrogen bonds with phosphate ions and/or crystalline water in the hydrated layer. These specific bonds may stabilize the bent structure of iminodicarboxylate ions and diglycolate ions in the OCP crystal. The bent structures of incorporated carboxylate ions will be elucidated using highly advanced methods, such as synchrotron radiation, in a future work. In addition, the calculation of d_{100}(cal.) using eqn (1) is based on the assumption that the main chain of carboxylate ions is parallel to the *a*-axis direction. However, because the $\Delta d_{100}/L$ values of IDAA and DGA for the main phase were −50.1% and −23.6%, respectively, and these values are particularly large, this assumption may not be applied. By contrast, the absolute values of $\Delta d_{100}/L$ for the minor phase of OCP with incorporated iminodicarboxylate ions and diglycolate ions were similar to those of OCP with incorporated glutarate ions, suggesting that the main chain of these carboxylate ions was parallel to the *a*-axis direction, as previously considered. In the case of TDGA, OCP with incorporated thiodiglycolate ions was not obtained. Nevertheless, if TDGA-incorporating OCP could be obtained, its value of d_{100} is expected to be approximately 2.27 nm according to eqn (1). Although previous studies demonstrated the guest selectivity of OCP, the physicochemical characteristics that determine which carboxylate ions can be incorporated into OCP were unclear. In this study, examining carboxylic acids with similar chemical structures, we found three carboxylic acids that were incorporated into OCP, as well as one carboxylic acid that could not be incorporated into OCP. Therefore, we investigated whether the dissociation constant, which can be used as an indicator of the physicochemical properties of carboxylic acids, controls the incorporation of carboxylate ions into OCP. Fig. 9 shows the pK_{a1} values of GA, IDAA, DGA, and TDGA plotted *versus* their pK_{a2} values. These values are presented in Table S1 in the SI. It is important to discuss the validity of the calculations. For this purpose, the values of pK_{a1} and pK_{a2} of GA reported in the literature[59] were compared with the values calculated in this study. The literature pK_{a1} and pK_{a2} values and our calculated values for GA are almost the same. Hence, the calculated values used in this study are most likely reasonable. Consideration of the XRD, FTIR, and dissociation constant results reveals an interesting insight. In this study, the incorporation of four carboxylic acids with similar molecular structures into OCP was investigated. The carboxylic acid that could not be incorporated into OCP, namely TDGA, exhibited an intermediate dissociation constant among these carboxylic acids.

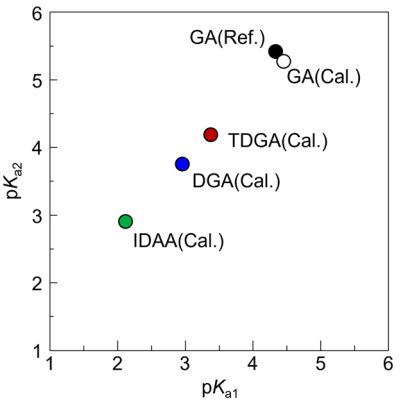

Fig. 9 Plot of pK_{a1} *vs.* pK_{a2} values of GA, IDAA, DGA, and TDGA. "Cal." means calculated values and "Ref." means the values cited from ref. 59.

Although several physicochemical indices can describe the properties of carboxylic acids, such as dissociation constant, molecular weight, molecular size, and hydrophilicity/hydrophobicity, considering the formation process of OCP with incorporated carboxylate ions, it is likely necessary to consider the stability constant of the carboxylate ion–calcium ion complex as one of the factors controlling the ability of carboxylate ions to be incorporated into OCP. Furthermore, if the incorporation of carboxylate ions is regarded as a competitive reaction with the incorporation of phosphate ions, both thermodynamic and kinetic considerations may be necessary. The results of this study clearly suggest that the dissociation constant of carboxylic acids does not significantly influence their ability to be incorporated into the OCP crystal. Therefore, additional research is necessary to elucidate the key physicochemical factors governing the ability of carboxylic acids to be incorporated into OCP. Although this study focused on OCP incorporating carboxylate ions, the fundamental knowledge gained here is expected to contribute to elucidating the formation mechanism of inorganic crystals occluding organic nanoparticles,[60–64] which has recently attracted attention.

Conclusions

In this study, OCP with incorporated carboxylate ions, which can be considered as a supra-ceramic, was synthesised in aqueous solutions of glutaric acid and its derivatives to investigate whether these carboxylic acids can be incorporated into the OCP crystal. The following results were obtained:

1. IDAA and DGA can be incorporated into OCP.
2. TDGA cannot be incorporated into OCP.
3. Considering findings 1 and 2 above and the calculated dissociation constants (pK_{a1} and pK_{a2}) of the carboxylic acids,

it is concluded that the dissociation constant of the carboxylic acid has little effect on its ability to be incorporated into OCP.

Although several factors that may influence the incorporation of carboxylic acids into OCP remain to be investigated, the finding that the dissociation constant of carboxylic acids is unlikely to affect their incorporation into the OCP crystal represents a step forward in our understanding of OCP chemistry and contributes to understanding the mechanism underlying the guest selectivity of OCP. Future research should focus on uncovering the mechanism of the guest selectivity of OCP by systematically studying the physicochemical properties of carboxylic acids, aside from their dissociation constants, as well as through comprehensive thermodynamic and kinetic analyses.

Author contributions

Taishi Yokoi: investigation, conceptualization, writing – original draft, writing – review & editing, visualization, project administration, and funding acquisition. Masakazu Kawashita: supervision and writing – review & editing.

Conflicts of interest

There are no conflicts to declare.

Data availability

The data supporting this article have been included as part of the supplementary information (SI). Supplementary information is available. See DOI: https://doi.org/10.1039/d5dt03031e.

Acknowledgements

We thank Mr Masahiro Watanabe for his experimental support. This work was partially supported by JSPS KAKENHI (grant no. 25H01648) and the Laboratory for Biomaterials and Bioengineering, Institute of Integrated Research, Institute of Science Tokyo (Project "Design & Engineering by Joint Inverse Innovation for Materials Architecture") of the Ministry of Education, Culture, Sports, Science, and Technology (MEXT), Japan.

References

1 S. Zhu, H. Xu, M. Yang, X. Yuan, W. Cui, N. Zhao, Y. Wei and B. Ying, *ACS Appl. Mater. Interfaces*, 2025, **17**, 55909–55922.
2 W. Xu, W. Guo, L. Liao, C. Xie, J. Cui, Q. Mei, S. Li, J. Wu, Z. Luo, Q. Zhang, X. Tang and G. Tan, *J. Am. Chem. Soc.*, 2025, **147**, 34804–34812.
3 Z. Wei, Y. Yu, A. Feng and H. Zhang, *ACS Appl. Mater. Interfaces*, 2025, **17**, 52172–52185.
4 H. Wang, C. Li, Z. Xiao, H. Xue, Z.-H. Dong, K. Yang, N. Zhang, Y. Lin, Y. Deng, Z. Lin, E. Li, Y. Liu, Z. Pu, Y. Bai, Z. Liu, H. Wang, C. Zhang, Z. Li, Y. Niu, B. Zhang, B. Nan, H. Lin, X. Liu and M. Zhang, *J. Am. Chem. Soc.*, 2025, **147**, 35355–35366.
5 J. Shi, P. Gong and J. Yao, *Cryst. Growth Des.*, 2025, **25**, 7200–7207.
6 F. V. Sainudeen, G. Behera, A. Alam and K. R. Balasubramaniam, *Inorg. Chem.*, 2025, **64**, 18687–18695.
7 S. Mattioni, Y. Asensio, P. Solokha, L. Olano-Vegas, M. Prato, S. De Negri, M. Gobbi, F. Casanova, A. Mateo-Alonso, L. E. Hueso and B. Martín-García, *ACS Appl. Mater. Interfaces*, 2025, **17**, 53745–53756.
8 H. Liao, J. Sun, X. Wang, Q. Tong, T. Liu, W. Zou and L. Dong, *Inorg. Chem.*, 2025, **64**, 17448–17458.
9 P. O. Adelani, J. E. S. Szymanowski, C. B. Gaster and C. E. Chamberlain, *Cryst. Growth Des.*, 2025, **25**, 8108–8114.
10 P. Acharyya, K. Pal, X. Shen, B. Zhang, B. Raveau, S. Passuti, P. Boullay, P. Lemoine, B. Malaman, C. Candolfi, A. Renaud, X. Zhou, T. Barbier and E. Guilmeau, *J. Am. Chem. Soc.*, 2025, **147**, 25806–25814.
11 M. Mathew, W. E. Brown, L. W. Schroeder and B. Dickens, *J. Crystallogr. Spectrosc. Res.*, 1988, **18**, 235–250.
12 W. E. Brown, J. P. Smith, J. R. Lehr and A. W. Frazier, *Nature*, 1962, **196**, 1050–1055.
13 H. Monma, *Bull. Chem. Soc. Jpn.*, 1984, **57**, 599–600.
14 H. Monma and M. Goto, *Bull. Chem. Soc. Jpn.*, 1983, **56**, 3843–3844.
15 T. Kataoka, A. Koga, S. Nishiyama, T. Yoshioka and S. Hayakawa, *Mater. Lett.*, 2025, **385**, 138188.
16 T. Yokoi, M. Watanabe and M. Kawashita, *J. Ceram. Soc. Jpn.*, 2024, **132**, 609–612.
17 Y. Sugiura, Y. Saito, E. Yamada and M. Horie, *Ceramics*, 2024, **7**, 796–806.
18 T. Kataoka, S. Nishiyama, E. Fujii, T. Yoshioka and S. Hayakawa, *Colloids Surf., A*, 2024, **693**, 134001.
19 T. Yokoi, M. Watanabe, F. Nakamura, H. Kimura-Suda, M. Shimabukuro and M. Kawashita, *Dalton Trans.*, 2023, **52**, 16586–16590.
20 T. Yokoi, M. Watanabe, T. Goto, S. Meng, T. Sekino, M. Shimabukuro and M. Kawashita, *Materials*, 2022, **16**, 64.
21 Y. Sugiura, E. Yamada and M. Horie, *Phys. Chem. Chem. Phys.*, 2023, **25**, 26640–26647.
22 Y. Sugiura, E. Yamada and M. Horie, *Ceram. Int.*, 2023, **49**, 9719–9724.
23 Y. Sugiura and Y. Makita, *J. Cryst. Growth*, 2022, **583**, 126545.
24 Y. Tsunawaki, K. Sakamoto, S. Yamaguchi, M. Asakawa, Y. Yamaguchi, S. Mitsudo and T. Idehara, *J. Infrared, Millimeter, Terahertz Waves*, 2021, **42**, 409–415.
25 D. Laurencin, Y. Li, M. J. Duer, D. Iuga, C. Gervais and C. Bonhomme, *Magn. Reson. Chem.*, 2021, **59**, 1048–1061.

26 E. Davies, K. H. Müller, W. C. Wong, C. J. Pickard, D. G. Reid, J. N. Skepper and M. J. Duer, *Proc. Natl. Acad. Sci. U. S. A.*, 2014, **111**, E1354–E1363.
27 T. Yokoi, T. Goto, M. Hara, T. Sekino, T. Seki, M. Kamitakahara, C. Ohtsuki, S. Kitaoka, S. Takahashi and M. Kawashita, *Commun. Chem.*, 2021, **4**, 4.
28 K. Maeda, T. Motohashi, R. Ohtani, K. Sugimoto, Y. Tsuji, A. Kuwabara and S. Horike, *Sci. Technol. Adv. Mater.*, 2024, **25**, 2416384.
29 T. Yokoi, M. Watanabe and M. Kawashita, *Dalton Trans.*, 2024, **53**, 14163–14170.
30 T. Yokoi, M. Watanabe, Y. Wang, T. Goto, T. Sekino, M. Shimabukuro and M. Kawashita, *J. Ceram. Soc. Jpn.*, 2023, **131**, 701–707.
31 T. Yokoi, T. Goto, T. Sekino and M. Kawashita, *J. Ceram. Soc. Jpn.*, 2022, **130**, 337–340.
32 I. Yamada and M. Tagaya, *Colloid Interface Sci. Commun.*, 2019, **30**, 100182.
33 N. J. Crane, V. Popescu, M. D. Morris, P. Steenhuis and M. A. Ignelzi, *Bone*, 2006, **39**, 434–442.
34 Y. Sugai, R. Hamai, Y. Shiwaku, T. Anada, K. Tsuchiya, T. Kimura, M. Tadano, K. Yamauchi, T. Takahashi, H. Egusa and O. Suzuki, *Biomimetics*, 2025, **10**, 205.
35 R. Hamai, K. Tomitsuka, M. Okada, K. Tsuchiya, T. Kimura, S. Sakai, K. Yamauchi and O. Suzuki, *Dent. Mater. J.*, 2025, **44**, 414–426.
36 L. Xiao, Y. Shiwaku, R. Hamai, K. Baba, K. Tsuchiya, S. Imazato, K. Sasaki and O. Suzuki, *J. Biomed. Mater. Res., Part A*, 2023, **111**, 1006–1020.
37 K. Okuyama, Y. Shiwaku, R. Hamai, T. Mizoguchi, K. Tsuchiya, T. Takahashi and O. Suzuki, *Acta Biomater.*, 2022, **142**, 332–344.
38 S. Koyama, R. Hamai, Y. Shiwaku, T. Kurobane, K. Tsuchiya, T. Takahashi and O. Suzuki, *Sci. Technol. Adv. Mater.*, 2022, **23**, 120–139.
39 R. Hamai, S. Sakai, Y. Shiwaku, T. Anada, K. Tsuchiya, T. Ishimoto, T. Nakano and O. Suzuki, *Appl. Mater. Today*, 2022, **26**, 101279.
40 S. Hamada, Y. Mori, Y. Shiwaku, R. Hamai, K. Tsuchiya, K. Baba, I. Oizumi, R. Kanabuchi, N. Miyatake, T. Aizawa and O. Suzuki, *Clin. Orthop. Relat. Res.*, 2022, **480**, 2043–2055.
41 T. Kibe, A. Maeda-Iino, T. Takahashi, S. Kamakura, O. Suzuki and N. Nakamura, *J. Oral Maxillofac. Surg.*, 2021, **79**, 2462–2471.
42 T. Kawai, S. Kamakura, K. Matsui, M. Fukuda, H. Takano, M. Iino, S. Ishikawa, H. Kawana, T. Soma, E. Imamura, H. Kizu, A. Michibata, I. Asahina, K. Miura, N. Nakamura, T. Kibe, O. Suzuki and T. Takahashi, *J. Tissue Eng.*, 2020, **11**, 2041731419896449.
43 T. Kawai, O. Suzuki, K. Matsui, Y. Tanuma, T. Takahashi and S. Kamakura, *J. Tissue Eng. Regener. Med.*, 2017, **11**, 1641–1647.
44 T. Kawai, S. Echigo, K. Matsui, Y. Tanuma, T. Takahashi, O. Suzuki and S. Kamakura, *Tissue Eng., Part A*, 2014, **20**, 1336–1341.
45 J. L. T. Tan, M. Shimabukuro, A. Tsuchiya, W. M. R. L. K. Wijekoon, R. Kishida, M. Kawashita and K. Ishikawa, *Ceram. Int.*, 2025, **51**, 19963–19972.
46 S. Takeda, A. Tsuchiya, M. Moriyama and K. Ishikawa, *Dent. Mater. J.*, 2025, **44**, 233–240.
47 K. Shibahara, K. Hayashi, Y. Nakashima and K. Ishikawa, *Biomater. Adv.*, 2025, **166**, 214026.
48 K. Hayashi, E. Teramoto, A. N. T. Alashkar, Z. Lou, M. Moriyama and K. Ishikawa, *ACS Appl. Mater. Interfaces*, 2025, **17**, 33340–33356.
49 P. Freitas, J. L. T. Tan and K. Ishikawa, *Materialia*, 2025, **42**, 102441.
50 S. Takeda, A. Tsuchiya, M. Moriyama and K. Ishikawa, *Ceram. Int.*, 2024, **50**, 53544–53551.
51 K. Hayashi, C. Zhang, A. N. T. Alashkar and K. Ishikawa, *ACS Appl. Mater. Interfaces*, 2024, **16**, 45956–45968.
52 K. Hayashi, R. Kishida, A. Tsuchiya and K. Ishikawa, *Adv. Healthcare Mater.*, 2024, **13**, e2303245.
53 K. Hayashi, T. Yanagisawa, R. Kishida, A. Tsuchiya and K. Ishikawa, *Comput. Struct. Biotechnol. J.*, 2023, **21**, 2514–2523.
54 H. Monma, *Gypsum Lime*, 1992, **237**, 108–114.
55 A. K. Rappe, C. J. Casewit, K. S. Colwell, W. A. Goddard and W. M. Skiff, *J. Am. Chem. Soc.*, 1992, **114**, 10024–10035.
56 https://avogadro.cc/.
57 M. Marković, B. O. Fowler and W. E. Brown, *Chem. Mater.*, 1993, **5**, 1406–1416.
58 T. Yokoi and M. Kawashita, *Materials*, 2021, **14**, 2703.
59 *Dissociation Constants of Organic Acids in Aqueous Solution*, ed. G. Kortüm, W. Vogel and K. Andrussow, Butterworths, London, 1961.
60 J. Zhang, B. Xiong, Z. Fu, Y. Ning and D. Li, *Small*, 2023, **19**, 2207843.
61 Y. Ning, S. P. Armes and D. Li, *Macromol. Rapid Commun.*, 2022, **43**, 2100793.
62 Y. Ning and S. P. Armes, *Acc. Chem. Res.*, 2020, **53**, 1176–1186.
63 Y. Ning, L. Han, M. J. Derry, F. C. Meldrum and S. P. Armes, *J. Am. Chem. Soc.*, 2019, **141**, 2557–2567.
64 Y.-Y. Kim, K. Ganesan, P. Yang, A. N. Kulak, S. Borukhin, S. Pechook, L. Ribeiro, R. Kröger, S. J. Eichhorn, S. P. Armes, B. Pokroy and F. C. Meldrum, *Nat. Mater.*, 2011, **10**, 890–896.